

Revisiting the Anodic Dissolution of Pure Iron in Strong Acids

Mohiedin Bagheri Hariri, Bruce Brown, and Srdjan Nestic

Institute for Corrosion and Multiphase Technology
Department of Chemical & Biomolecular Engineering
Ohio University
342 West State Street
Athens, Ohio, 45701
USA

ABSTRACT

The goal of the research reported herein was to accomplish a quantitative mechanistic analysis of iron dissolution in strong acid in a potential range in the proximity of its open circuit potential (OCP), leading to articulation of a revised narrative of BDD[†] mechanism for iron dissolution; additional mechanistic pathways were postulated in addition to the hypothesized mechanisms of BDD and Heusler. Thirty-eight different pathways were investigated here and theoretical Butler-Volmer equations were written for each. The kinetic consequences of each pathway and the corresponding theoretical values of the main kinetic parameters were determined, and the theoretical outcomes were compared to the experimental observations. It was found that in strong acids ($\text{pH} \leq 4$) in the potential range of ± 50 mV vs. OCP, the mechanism of iron dissolution agrees well with three pathways, and all three were explainable within the same framework of BDD mechanism, where the reaction of OH^- with iron produces the adsorbed intermediate FeOH_{ads} . One single dissolution pathway which corresponds to the conversion of FeOH_{ads} to $\text{Fe(II)}_{\text{sol}}$ is dominant in the potential range adjacent to the OCP. Near OCP the effect of hydrogen reduction was taken into account using the linearity of the cathodic potentiodynamic branch to approximately extract the pure anodic data points from both anodic and cathodic sweeps.

Key words: Anodic dissolution, Iron, Strong Acid

INTRODUCTION

Reviewing literature related to corrosion research brings to light the importance of understanding the mechanisms involved, and how this is essential to aid in development of mathematical models for corrosion prediction. The current research documents possible mechanisms for the dissolution of pure iron in strong acid in a potential range in the potential range of ± 50 mV vs. OCP, providing explanations for corrosion engineers and researchers working with mild steel. Prediction of corrosion rate relies on the precise understanding of the anodic and cathodic processes at the metal surface in the potential range close to the OCP. In the case of iron dissolution, not far from OCP, there are two common mechanisms in strong acids ($\text{pH} \leq 4$) reported in the literature; namely, the “catalytic mechanism” proposed by Heusler

[†]BDD stands for co-authors’ names Bockris, Drazic and Despic who proposed the mechanism of iron dissolution: Bockris, J.O., Drazic, D. & Despic, *Electrochimica Acta* 4, 325–361 (1961).

© 2022 Association for Materials Protection and Performance (AMPP). All rights reserved. No part of this publication may be reproduced, stored in a retrieval system, or transmitted, in any form or by any means (electronic, mechanical, photocopying, recording, or otherwise) without the prior written permission of AMPP.

Positions and opinions advanced in this work are those of the author(s) and not necessarily those of AMPP. Responsibility for the content of the work lies solely with the author(s).

et al.¹, and the “consecutive mechanism” postulated by Bockris, et al.² which is also known as “BDD mechanism”. Heusler’s model is based on the second order dependence on OH⁻ ions and the anodic Tafel slope of 30 mV/decade, while BDD mechanism predicts a first order of dependency on OH⁻ and an anodic Tafel slope of 40 mV/decade. Over a wider range of overpotentials far from the OCP, Keddum, et al., reported that iron dissolution occurs through three different but interrelated dissolution paths in which four adsorbed intermediates are involved in seven elementary steps.³ Bockris’ approach^{2,4} for elucidation of the mechanism near the OCP was methodical in terms of utilizing the Butler-Volmer equation as a means to reasonably deduce the mechanism since it immediately provides the metrics to prove, or disprove, a particular hypothesis.

In the present study, Bockris’ style analysis of the Butler-Volmer equation for understanding the mechanism of iron dissolution is revisited. Additional mechanistic pathways for the occurrence of iron dissolution in addition to those postulated models of BDD and Heusler are presented. For all proposed pathways, the theoretical Butler-Volmer was derived, and the corresponding theoretical consequences of each pathway were computed and compared with the experimental metrics. Finally, the most likely mechanism for iron dissolution in strong acids (pH ≤ 4) was established for the potential ranges in close proximity to the OCP. Measurements of OCP, linear polarization resistance (LPR), and potentiodynamic sweeps were utilized to collect the experimental metrics. The present study is limited to the potential ranges not far from OCP in order to validate the existing mechanistic interpretation and to find if the proposed pathway involving formation and dissolution of FeOH_{ads} is actually the predominant path or not. Mechanisms at higher overpotentials far from OCP are not discussed in this study.

EXPERIMENTAL PROCEDURE

Equipment

Figure 1 depicts the 2-liter glass cell (with a rotating cylinder electrode (RCE) as working electrode, four platinum-coated titanium mesh counter electrodes, and Ag/AgCl reference electrode) which was used to investigate corrosion in this work. RCE specimen was 99% pure iron. The four counter electrodes were used to provide a more symmetric current distribution around the rotating working electrode. All RCE specimens were polished to 0.25-micron, rinsed with deionized (DI) water and isopropanol, sonicated for 5 minutes, and air dried. Prior to each measurement the OCP was monitored for at least 20 minutes to ensure it was stable. The anodic and cathodic polarization curves were collected separately, always starting at OCP, and were corrected for the effect of IR drop due to the 0.15 M Na₂SO₄ electrolyte. The solution resistance was determined using LPR and electrochemical impedance spectroscopy (EIS) measurements, its mean value being used. EIS measurements were performed at OCP in a frequency range from 100 kHz to 1 Hz at 10 points/decade. All potentiodynamic sweeps were collected at a 0.125 mV/s scan rate with sampling rate of 1 s⁻¹. LPR measurements were performed at the same scan rate over a potential range of ±5 mV vs. OCP. A Solartron 1470E[‡] potentiostat was used for LPR, OCP and potentiodynamic measurements. The OCP was monitored for 5 min prior to each measurement. The EIS measurement was done using a VersaSTAT3[§] potentiostat instrument.

[‡] Trade Name

[§] Trade Name

© 2022 Association for Materials Protection and Performance (AMPP). All rights reserved. No part of this publication may be reproduced, stored in a retrieval system, or transmitted, in any form or by any means (electronic, mechanical, photocopying, recording, or otherwise) without the prior written permission of AMPP.

Positions and opinions advanced in this work are those of the author(s) and not necessarily those of AMPP. Responsibility for the content of the work lies solely with the author(s).

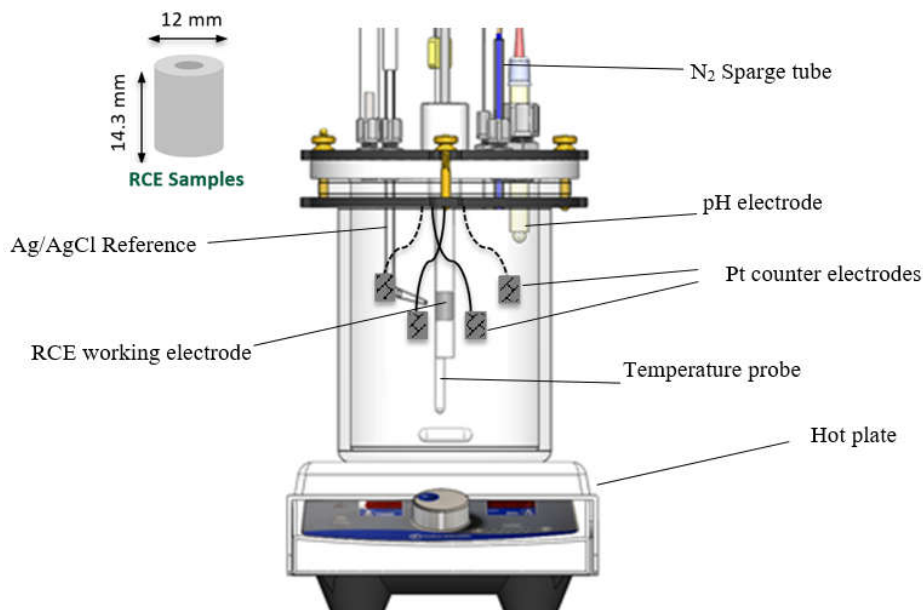


Figure 1. Schematic representation of the experimental cell setup.

Experimental Conditions

Table 1 summarizes the experimental conditions used in this study.

Table 1. Experimental conditions

Parameters	Values
pH	2.0, 2.5, 3.0, 3.5, and 4.0
Temperature	30°C
RCE Rotational Speed	2000 rpm
Electrolyte	0.15 M Na ₂ SO ₄
Setup	2L Glass cell
RCE working electrode	99% pure Fe
pN ₂	0.97 bar

The 0.15 M Na₂SO₄ supporting electrolyte was purged for about 2 hr with N₂ gas prior and during each experiment throughout this study. The temperature was controlled (to ±0.5°C) using a HH11B OMEGA** thermometer. The pH was adjusted using 0.1 M H₂SO₄ or 0.1 M NaOH solution as necessary.

RESULTS AND DISCUSSION

Speculation of the Possible Pathways of Iron Dissolution

The overall anodic half-reaction for iron dissolution, i.e., $\text{Fe} \rightarrow \text{Fe}^{2+} + 2\text{e}^-$, is a multistep reaction. Speculation of the possible pathways for a particular overall reaction is not a random affair, and several diagnostic criteria must be utilized to elucidate the mechanistic pathway. Table 2 summarizes the hypothesized pathways for iron dissolution in strong acids. Mechanisms (a) through (e) are taken from Bockris & Reddy (1970)⁴, and mechanism (f) represents the mechanism proposed by Heusler.¹ The rest of the schemes, i.e., pathways (g) through (s) and (a') through (s') are additional mechanistic speculations made in the present study. The goal was to test the feasibility of iron dissolution via other possible pathways. Other so-called branching pathways were also explored.⁵ Mechanisms (a') through (s') indicate the branching process for the corresponding elementary steps (a) through (s), respectively.

** Trade Name

© 2022 Association for Materials Protection and Performance (AMPP). All rights reserved. No part of this publication may be reproduced, stored in a retrieval system, or transmitted, in any form or by any means (electronic, mechanical, photocopying, recording, or otherwise) without the prior written permission of AMPP.

Positions and opinions advanced in this work are those of the author(s) and not necessarily those of AMPP. Responsibility for the content of the work lies solely with the author(s).

variation of the anodic exchange current density with respect to the concentration of OH⁻ ion ($p_{OH^-}^i$) was calculated for each scheme (Equation 1).

$$p_{OH^-}^i = \frac{\partial \log(i_{0,a})}{\partial \log(C_{OH^-})} \quad (1)$$

Additionally, the dependency of corrosion potential on OH⁻ ion ($E_{OH^-}^i$) was computed for each scheme (Equation 2).

$$E_{OH^-}^i = \frac{\partial E_{corr}}{\partial \log(C_{OH^-})} \quad (2)$$

Table 3 summarizes the computed theoretical outcomes corresponding to each scheme. The detailed approach for computing the kinetic parameters is explained by Bockris & Reddy (1970)⁴. The values of cathodic Tafel slopes were measured to be greater than or equal to 120 mV/decade under our experimental conditions. This study is based on the assumption that there is no corrosion product forming at the electrode surface. In addition, all mechanistic pathways have been written within the range of potential where the mass-transfer limitation is insignificant. In this study, all reaction pathways are written within the range near the corrosion potential, i.e., potential range not far from OCP.

Table 3. Theoretical predictions of kinetic parameters computed for different mechanistic pathways at 303 K

Mechanism	β_a^i (mV/decade)	$p_{OH^-}^i$	$E_{OH^-}^i$ (mV/decade)	Mechanism	β_a^i (mV/decade)	$p_{OH^-}^i$	$E_{OH^-}^i$ (mV/decade)
a	60	2	-90	a'	30	0.5	-30
b	30	1	-30	b'	30	1	-30
c	60	1	-60	c'	30	1	-60
d	40	2	-90	d'	30	3	-120
e	40	1	-60	e'	30	1	-60
f	30	2	-60	f'	20	1	-40
g	24	0	-20	g'	30	1	-60
h	120	1	-40	h'	30	1	-40
i	60	0	-30	i'	30	3	-120
j	60	0	-30	j'	30	3	-120
k	24	2	-45	k'	15	3	-60
l	24	1	-30	i'	60	0	-15
m	40	1	-30	m'	30	2	-90
n	120	0	-60	n'	60	0	-60
o	60	0	-30	o'	60	0	-30
p	30	0	-15	p'	20	2	-45
q	30	0	-30	q'	30	0	-30
r	20	1	-30	r'	15	3	-30
s	24	4	-75	s'	15	3	-60

Experimental Observations

With the theoretical values known for each of the mechanistic pathways (Table 3), experimental metrics were collected to either validate or disprove a particular scheme.

Dependency of E_{corr} on pH.

Four different experimental metrics were gathered; namely, the anodic Tafel slope (β_a), cathodic Tafel slope (β_c), order of reaction with respect to OH⁻ (For each mechanistic scheme, the theoretical Butler-Volmer equation was computed. β_a^i and β_c^i are the anodic and the cathodic Tafel slopes for a specific mechanism, respectively. $p_{OH^-}^i$ or the theoretical variation of the anodic exchange current density with respect to the concentration of OH⁻ ion (

$p_{OH^-}^i$) was calculated for each scheme (Equation 1), and dependency of corrosion potential on the concentration of OH^- in the bulk solution (Additionally, the dependency of corrosion potential on OH^- ion ($E_{OH^-}^i$) was computed for each scheme (Equation 2). Figure 2 shows the variation of corrosion potential as a function of time for iron in 0.15 M Na_2SO_4 solution at four different pH values.

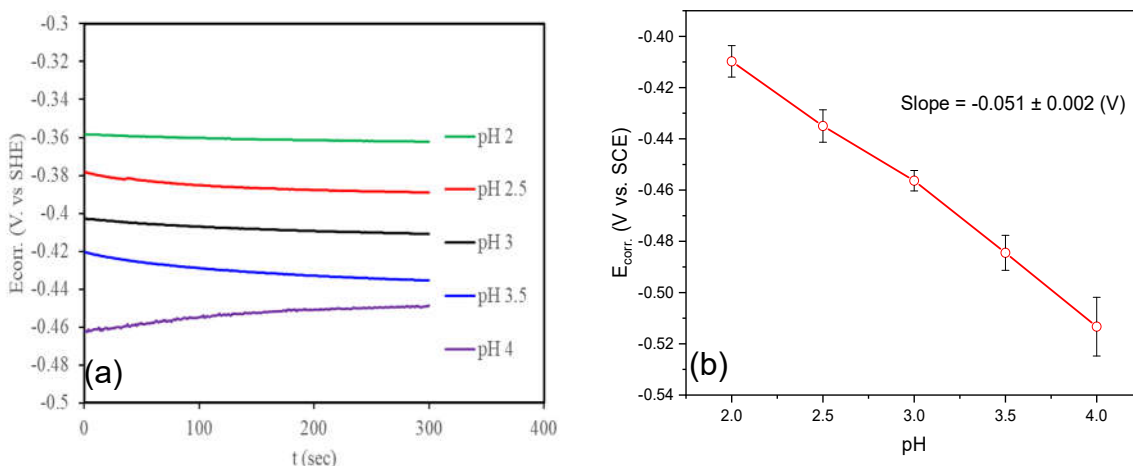


Figure 2. (a) OCP variation over time, and (b) dependency of corrosion potential on pH for pure iron in 0.15 M Na_2SO_4 solution, at 30°C, sparged with nitrogen.

The dependency of corrosion potential on pH was measured to be -51 ± 2 mV/decade.

Determining the anodic Tafel slopes.

Often times, especially when the pH is lower than 4, the linear portion of the cathodic Tafel slope can be obtained relatively easily from potentiodynamic sweeps, however, there is no reasonable linearity for the anodic branch, which is mainly due to the rapid kinetics of anodic dissolution, or dominance of adsorption phenomena that might cause undesirable disturbances in the linear Tafel range.⁹ Near OCP, the anodic Tafel slope can include interference by the cathodic reaction. Hence, it is important to take into consideration the impact of cathodic current on anodic sweeps and vice versa. In the example given in Figure 3, the cathodic and anodic sweeps were collected separately, and they both contain net currents. At potentials where the anodic current density is negligible as compared to the cathodic current density (at least 2 orders of magnitude less), a linear portion of the cathodic sweep was chosen (dotted box) and cathodic Tafel calculated to be -185 mV/decade. The values along this cathodic Tafel line (black line in Figure 3) were used to extract the pure cathodic current density ($i_{cathodic}$) near the OCP to determine the values of pure anodic current density (i_{anodic}). To extract the linear range of the anodic branch, the anodic current will be the net current minus the pure cathodic current.¹⁰

$$i_{anodic} = i_{net} - i_{cathodic} \quad (3)$$

By subtracting the net current from the cathodic current (the black solid line), two sets of anodic data points could be obtained. One set of anodic data points were obtained from the anodic sweep according to Equation (4), and the other ones were computed from the net cathodic curve according to Equation (5):¹⁰

$$i_{anodic}^1 = i_{anodic_net} - i_{cathodic} \quad (4)$$

$$i_{anodic}^2 = i_{cathodic_net} - i_{cathodic} \quad (5)$$

This way, two different anodic Tafel slopes are extracted adjacent to OCP. One anodic Tafel slope is calculated from the cathodic branch and the other one is determined using the anodic branch. Hence, using the steady state potentiodynamic measurements from each experiment, the β_a will be reported as the average between these two values. Figure 3 represents this approach for anodic Tafel slope determination for pure iron in strong acidic solution with 0.15 M Na₂SO₄ electrolyte (pH 2) at 30°C. The regions that are shown in grey, red and blue indicate the data points that are used for determining the cathodic Tafel slope, anodic Tafel slope on the cathodic branch, and anodic Tafel slope on the anodic branch, respectively.

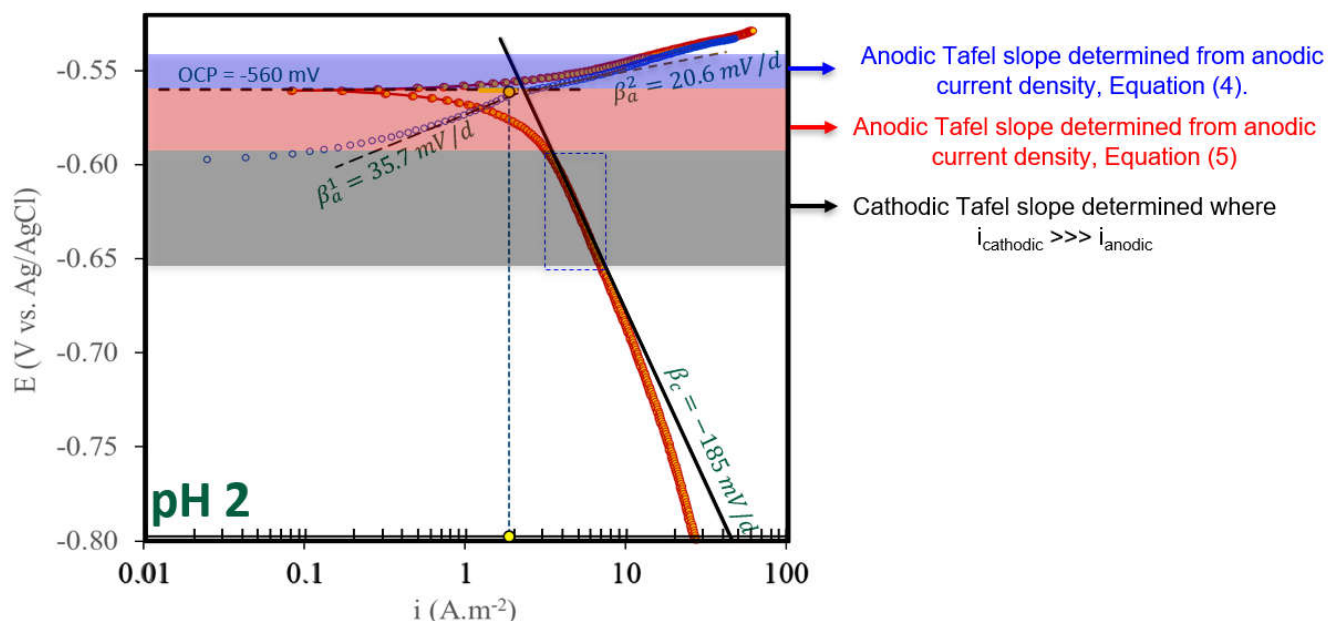


Figure 3. Determination of the anodic Tafel slope using the linearity of the cathodic sweep for pure iron in strong acid 0.15 M Na₂SO₄ electrolyte at 30°C, pH 2.0, sparged with nitrogen.

The anodic Tafel slope for iron dissolution at pH 2 was measured to be in the range of 20.6 – 35.7 mV/decade (average $\beta_a = 28.2$ mV/decade, error of ± 7.6 mV/decade). The R_p value under the studied experimental condition at pH 2 was measured to be $5.5 \times 10^{-3} \Omega \cdot \text{m}^2$. Knowing the β_a , the corrosion current density (i_{corr}) was determined to be $1.8 \pm 0.6 \text{ A} \cdot \text{m}^{-2}$. The intersection of the cathodic line with the point where the two anodic Tafel lines meet each other lies on the OCP (shown in yellow). A similar approach was followed to determine the range of the anodic Tafel slope for pH 2.5, 3.0, 3.5, and 4.0. Table 4 summarizes the anodic Tafel slopes (β_a), R_p , and i_{corr} values obtained from the potentiodynamic analysis, as explained above. From this analysis, the anodic Tafel slope was defined to be 38.2 ± 10 mV/decade. The error of ± 10 mV/decade means that this metric needs to be used carefully when it comes to comparison against theory. As the error for experimental anodic Tafel slope is relatively high, when comparing experimental values with the corresponding theoretical predictions, first the parameters other than β_a will be assessed.

Table 4. Calculated values of β_a , R_p , and i_{corr} at different pHs in strong acid 0.15 M Na₂SO₄ solution, sparged with nitrogen, at 30 °C.

pH	β_a (mV/decade)	R_p ($\Omega \cdot \text{m}^2$)	i_{corr} (A/m^2)
2.0	28.1 ± 7.5	5.5×10^{-3}	1.8 ± 0.6
2.5	47.5 ± 11.7	5.6×10^{-3}	3.0 ± 0.6
3.0	36.4 ± 12.3	5.2×10^{-3}	2.5 ± 0.7
3.5	40.6 ± 15.8	5.4×10^{-3}	2.7 ± 0.9
4.0	38.8 ± 6.7	6.4×10^{-3}	2.2 ± 0.3

Variation of $i_{0,\text{anodic}}$ as a Function of pH

To calculate the anodic exchange current density, the averaged Tafel line was extrapolated to a standard reversible potential for iron dissolution ($E_{0,\text{rev.anodic}}$ referenced from Bockris, et al. (1961)²) near -680 mV vs. Ag/AgCl. The intersection of the extrapolated line with the reversible potential is defined as the exchange current density of iron dissolution ($i_{0,\text{anodic}}$). Figure 4 shows this method of determining $i_{0,\text{anodic}}$ for pure iron in 0.15 M Na_2SO_4 electrolyte (pH 2) at 30°C.

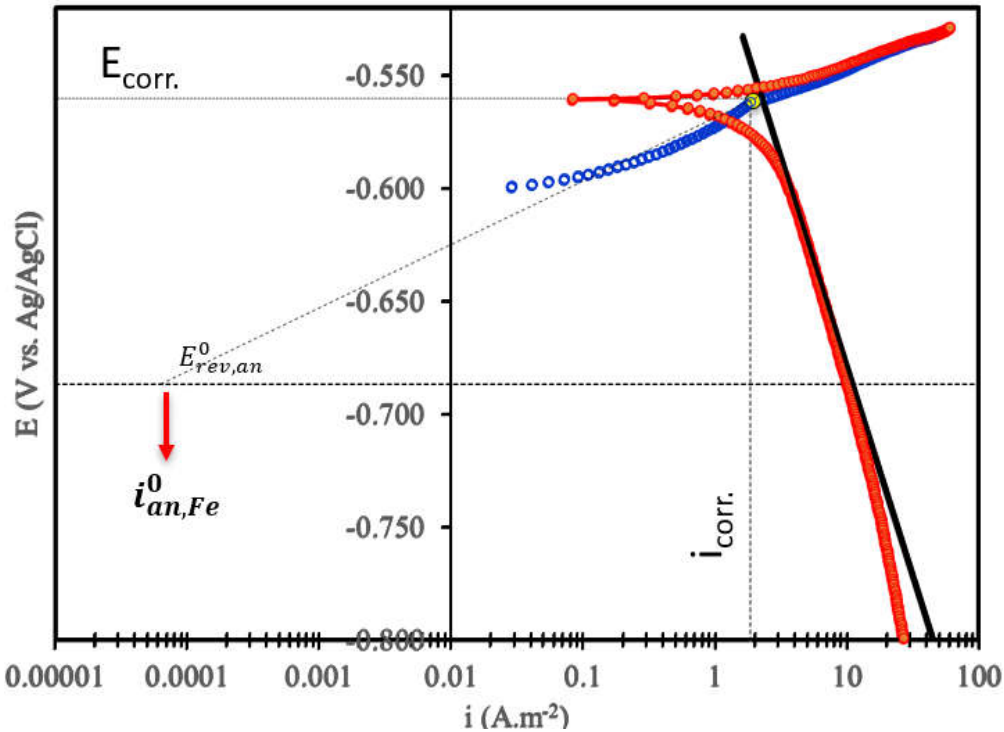


Figure 4. (a) Determining $i_{0,\text{anodic}}$ for pure iron in strong acid at pH 2 at 30°C, in 0.15 M Na_2SO_4 solution sparged with nitrogen, (b) Variation of as a function of concentration of OH^- for pure iron in strong acid at 30°C, in 0.15 M Na_2SO_4 solution sparged with nitrogen.

The procedure shown in Figure 4 to define the $i_{0,\text{anodic}}$ associated with the averaged anodic Tafel line for pH 2.0 was repeated for similar experiments at pH 2.5, 3.0, 3.5, & 4.0. The exact value of the reversible potential as the reference potential for determining the exchange current density does not matter but the same potential used at pH 2 was required to be used for all analysis. To find the dependency of $i_{0,\text{anodic}}$ on pH, the log of the exchange current density vs. the log of concentration of hydroxide (OH^-) was plotted (Figure 5) to determine the $p_{\text{OH}^-}^i$ as in Equation 1. According to this analysis, in strong acid for pure iron at $\text{pH} \leq 4$, the order of reaction dependency with respect to OH^- was found to be about 1.42 ± 0.3 (Figure 5). The same slope will be obtained even if a slightly different reversible potential value is used for calculating the anodic exchange current density.

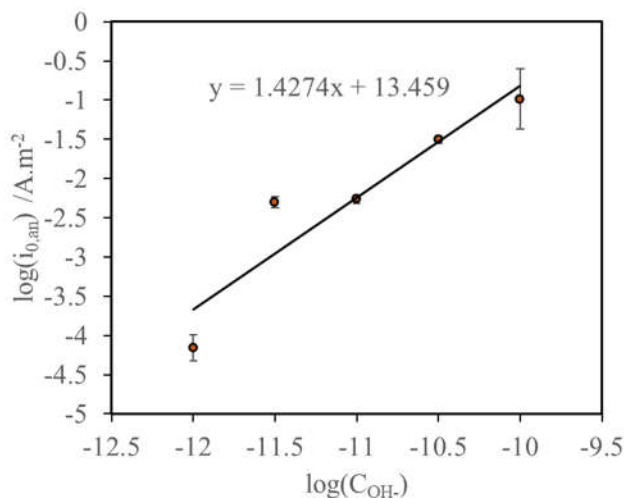


Figure 5. Variation of $i_{0,\text{anodic}}$ as a function of concentration of OH^- for pure iron in strong acid at 30°C , in $0.15\text{ M Na}_2\text{SO}_4$ solution sparged with nitrogen.

Comparing Theory vs. Experiment

After collection of experimental data, comparisons with theoretical predictions as previously summarized in Table 3 can then be made in order to determine the most plausible mechanisms out of the aforementioned 38 mechanistic schemes. It was found that the most consistent exists for mechanisms (e), (e'), (c'), and (g'). Table 5 represent these most plausible schemes.

Table 5. The most plausible mechanisms

e	$\text{Fe} + \text{H}_2\text{O} \leftrightarrow \text{FeOH}_{\text{ads.}} + \text{H}^+ + \text{e}^-$ $\text{FeOH}_{\text{ads.}} \xrightarrow{\text{rds}} \text{FeOH}_{\text{ads.}}^+ + \text{e}^-$ $\text{FeOH}_{\text{ads.}}^+ + \text{H}^+ \leftrightarrow \text{Fe}^{2+} + \text{H}_2\text{O}$	e'	$\text{Fe} + \text{H}_2\text{O} \leftrightarrow \text{FeOH}_{\text{ads.}} + \text{H}^+ + \text{e}^-$ $\text{FeOH}_{\text{ads.}} \xrightarrow{\text{rds}} \text{FeOH}_{\text{ads.}}^+ + \text{e}^-$ $\text{FeOH}_{\text{ads.}}^+ \xrightarrow{\text{des}} \text{FeOH}^+$ $\text{FeOH}^+ + \text{H}^+ \leftrightarrow \text{Fe}^{2+} + \text{H}_2\text{O}$
c'	$\text{Fe} + \text{OH}^- \xrightarrow{\text{rds}} \text{FeOH}_{\text{ads.}}^+ + 2\text{e}^-$ $\text{FeOH}_{\text{ads.}}^+ \xrightarrow{\text{des}} \text{FeOH}^+$ $\text{FeOH}^+ \leftrightarrow \text{Fe}^{2+} + \text{OH}^-$	g'	$\text{Fe} + \text{FeOH}_{\text{ads.}} + \text{OH}^- \leftrightarrow (\text{FeOH})_{2,\text{ads.}} + \text{e}^-$ $(\text{FeOH})_{2,\text{ads.}} \leftrightarrow (\text{FeOH})_{2,\text{ads.}}^+ + \text{e}^-$ $(\text{FeOH})_{2,\text{ads.}}^+ \xrightarrow{\text{rds}} \text{FeOH}_{\text{ads.}}^+ + \text{FeOH}_{\text{ads.}}$ $\text{FeOH}_{\text{ads.}}^+ \xrightarrow{\text{des}} \text{FeOH}^+$ $\text{FeOH}^+ \leftrightarrow \text{Fe}^{2+} + \text{OH}^-$

Mechanism (e) and mechanism (e')

Mechanisms (e) and (e') are assumed to be the same and mechanism (e') is basically written based on (e). Mechanism (e) is the BDD model for iron dissolution and (e') is the branched version of mechanism (e). Mechanism (e') takes place when the rate-determining step in mechanism (e) is divided into two sub-elementary steps. As a result, the number of electrons transferred after and during rate-limiting step changes leading to a decrease of anodic Tafel slope from 40 to 30 mV/decade. When the adsorption energy of the intermediates of $\text{FeOH}_{\text{ads.}}^+$ or $(\text{FeOH})_{2,\text{ads.}}^+$ is increased the rate of rate-determining step in mechanism (e) will be increased, while the rate of desorption step in mechanism (e') is decreased. Hence, the conversion of $\text{FeOH}_{\text{ads.}}$ to $\text{FeOH}_{\text{ads.}}^+$ will no longer be the rate-controlling step, instead $\text{FeOH}_{\text{ads.}}$ tends to first be converted to $\text{FeOH}_{\text{ads.}}^+$ before dissolving into the solution. Therefore, mechanism (e) will have a tendency to branch (as predicted in mechanism (e')).⁵

Feasibility of mechanism (c')

The branching process was first explained by Drazic⁵, who proposed the feasibility of the change in the position of the rate-determining step to a slow desorption step. These researchers claimed that depending on pH of the solution and the surface activity, a particular portion of the reaction may proceed through the direct $\text{FeOH}_{\text{ads}}^+$ path or via $\text{Fe}(\text{OH})_{2,\text{ads}}$ path (branching), leading to a reaction order with respect to OH^- between 1.6 and 1.8 (but < 2).⁵ Keddiam, et al.,³ and Schweickert, et al.,¹¹ also postulated the existence of similar branching processes. The probability of two electrons tunneling simultaneously across the metal-solution interface is so negligible that it has become well accepted that the mechanism excludes paths which would involve multiple electron transfers in one single step.¹² Simultaneous transfer of two electrons requires an activation energy much higher than that of a single electron transfer.^{4,12} Therefore, the possibility of mechanism (c') is expected to be much less than those of the other three pathways (e), (e'), and (g').

Comparison between mechanism (e') and (g')

As was just stated, mechanisms (e) and (e') are basically explaining the same principle for iron anodic dissolution, except that the later one assumes branching of the rds step in (e). Mechanism (e') is based on adsorption of one single FeOH_{ads} and its subsequent conversion to $\text{FeOH}_{\text{ads}}^+$ followed by its desorption into the solution. Similarly, mechanism (g') also conveys the same idea except that it describes dissolution through adsorption of two FeOH_{ads} and its conversion to two $\text{FeOH}_{\text{ads}}^+$ species. Mechanism (g') assumes that the dissolution starts by consuming adsorbed FeOH_{ads} acting as a catalyst. Mechanism (g') in this study is different from the scheme proposed by Heusler¹. Mechanism (g') is speculated for the first time and, after computational analysis, was found to result in reasonable kinetic predictions for the electrode reaction. Interestingly, it was found that mechanism (g') also explains the same scheme for iron dissolution as described in earlier works by Bockris, et al.² Pathways (e') and (g'), both produce the same species, through the same desorption rds step. Therefore, both mechanisms (e') and (g') are fundamentally similar explanations for iron's anodic dissolution, although (g') is a more complicated version of (e'). However, according to Occam's razor principle, between mechanism (e') and (g'), the simplest explanation should be considered as the preferred one. Hence, compared to mechanism (g'), the mechanism (e') is the more appropriate mechanistic pathway for explaining iron's oxidative dissolution in strong acid ($\text{pH} \leq 4$).

Table 6 shows the comparison between the experimental findings with theoretical predictions of pathways (e), (e'), (c'), and (g'). $p_{\text{OH}^-}^i$ is the dependency of anodic exchange current density with respect to the concentration of OH^- is computed based on theoretical Butler-Volmer equation.

Table 6. Comparison between experiment vs. theory for the most likely mechanisms for iron dissolution in strong acid ($\text{pH} \leq 4$).

Mechanism	β_a (mV/decade)	Order of dependency wrt. OH^-	Variation of E_{corr} wrt. OH^- (mV/dec)
Experimental Results	38.2 ± 10	1.42 ± 0.3	-51 ± 2
Mechanism (e)	40	1	-60
Mechanism (e')	30	1	-60
Mechanism (c')	30	1	-60
Mechanism (g')	30	1	-60

Both (e) and (e') mechanisms are valid

Both mechanisms (e) and (e') could reasonably predict the experimental observations, depending on the number of active sites available for intermediate adsorption.⁵ Mechanism (e) predicts an anodic Tafel slope of 40 mV/decade, while the branched version of mechanism (e), i.e. (e'), anticipates the anodic Tafel slope of 30 mV/decade. The occurrence of either pathway (e) or pathway (e') depends on the adsorption energy and the properties of the active surface of the electrode. The density of the active sites

© 2022 Association for Materials Protection and Performance (AMPP). All rights reserved. No part of this publication may be reproduced, stored in a retrieval system, or transmitted, in any form or by any means (electronic, mechanical, photocopying, recording, or otherwise) without the prior written permission of AMPP.

Positions and opinions advanced in this work are those of the author(s) and not necessarily those of AMPP. Responsibility for the content of the work lies solely with the author(s).

and the properties of the electrode surface can be changed due to heat treatment, cold work, strain, hydrogen adsorption, properties of the metallic interface, etc.¹³⁻¹⁵. By changing the solution pH, a slight change of the anodic Tafel slope has been also reported elsewhere¹⁶ especially at pH higher than 4. These change of the anodic Tafel slope from 40 to 30 mV/decade can be attained within the framework of the same mechanism (e), but only by changing the position of the rate-determining step due to the change of the number of the active sites on the electrode surface.

CONCLUSIONS

Anodic dissolution mechanisms for pure iron in strong acid media were revisited in the potential range of about ± 50 mV vs. OCP. The following conclusions are drawn:

1. The results indicated that the most probable pathways for iron dissolution are mechanisms (e), (e'), and (g), as listed in Table 5. For all three, the kinetic outcomes are close and within the range of experimental observations ($\text{pH} \leq 4$).
2. In some experimental cases, the difference from 40 mV/decade (similar to BDD mechanism) to 30 mV/decade was obtained. These changes are still explainable within the same framework of mechanism (e). Decrease in the anodic Tafel slope from 40 mV/decade to 30 mV/decade is not an indication of the change of the mechanism of anodic dissolution ($\text{pH} \leq 4$), as suggested by Heusler's mechanisms. Only the change in the position of the rate-determining step in the same reaction sequence is influencing the anodic Tafel value. These changes in anodic Tafel slope are explainable based on the original BDD mechanism (e).
3. In the vicinity of OCP, the dominant adsorbed intermediate that controls the dissolution of iron is most likely FeOH_{ads} , and the dissolution of FeOH_{ads} to the $\text{Fe(II)}_{\text{sol}}$ is the predominant pathway in the potential range close to the OCP.

REFERENCES

1. Heusler, K.E. Encyclopedia of Electrochemistry of the Elements vol. 9. Marcel Dekker, New York (1982).
2. Bockris, J.O., Drazic, D. & Despic, A.R. The Electrode kinetics of the deposition and dissolution of iron. *Electrochimica Acta* 4, 325–361 (1961).
3. Keddani, M., Mattos, O.R. & Takenouti, H. Reaction Model for Iron Dissolution Studied by Electrode Impedance. *J. Electrochem. Soc.* 128, 257-266 (1981).
4. Bockris, J. & Reddy, A.K.N. Modern Electrochemistry. 2, An introduction to and interdisciplinary area. Plenum Press, NY (1970).
5. Drazic, D.M. Iron and Its Electrochemistry in an Active State: Modern Aspects of Electrochemistry. Plenum Press, New York (1989).
6. Shock, E.L., Sassani, D.C., Willis, M. & Sverjensky, D.A. Inorganic species in geologic fluids: Correlations among standard molal thermodynamic properties of aqueous ions and hydroxide complexes., *Geochimica et Cosmochimica Acta* 61, 907-950 (1997).
7. Kim, S., Marrs, C., Nemas, M. & Jang, J.J.H. Solubility Model for Ferrous Iron Hydroxide, Hibbingite, Siderite, and Chukanovite in High Saline Solutions of Sodium Chloride, Sodium Sulfate, and Sodium Carbonate. *ACS Earth Space Chem.* 1, 647–663 (2017).
8. Fosbol, P.L., Thomsen, K. & Stenby, E.H. Review and recommended thermodynamic properties of FeCO_3 . *Corrosion Engineering, Science and Technology* 45, 115-135 (2013).
9. Poursaeed, A. Potentiostatic transient technique, a simple approach to estimate the corrosion current density and Stern–Geary constant of reinforcing steel in concrete. *Cement and Concrete Research* 40, 1451–1458 (2010).
10. Jones, D. A. Principles and Prevention of Corrosion 2nd ed. Prentice Hall, (1995).
11. Schweickert, H., Lorenz, W. J. & Friedburg, H. Impedance Measurements of the Anodic Iron Dissolution. *J. Electrochem. Soc.* 127, 1693-1701 (1980).

12. Appleby, A.J. Chemistry, electrochemistry and electrochemical applications. *Encyclopedia of Electrochemical power sources*, (2009).
13. Stansbury, E.E. & Buchanan, R. A. Fundamentals of Electrochemical Corrosion. *ASM International* (2000).
14. Aghaaminiha, M., Mehrani, R., Colahan, M., Brown, B., Singer, M., Netic, S., Vargas, S.M. & Sharma, S. Machine learning modeling of time-dependent corrosion rates of carbon steel in presence of corrosion inhibitors. *Corrosion Science* 193, 109904 (2021).
15. Aghaaminiha, M. Application of Molecular Simulations and Machine Learning Methods to Study Biological and Metallic Interfaces in Aqueous Environment. PhD Dissertation, *Ohio University*, (2021).
16. Sharifi Abdar, P., Bagheri Hariri, M., Kahyarian, A. & Netic, S. A revision of mechanistic modeling of mild steel corrosion in H₂S environments. *Electrochimica Acta* 382, 138231 (2021).